# Computational study of neutral and cationic pericondensed polycyclic aromatic hydrocarbons

Amit Pathak, Shantanu Rastogi *

*Department of Physics, D.D.U. Gorakhpur University, Gorakhpur 273 009, India*

**Abstract**

Quantum chemical calculations using Density Functional Theory are presented for small to medium sized pericondensed PAHs including some being reported for the first time. Bond lengths and charge distribution have been computed for these PAHs in both neutral and cationic forms. Upon ionization, significant change in fractional charge on atoms is present particularly for the outer carbon atoms. The charge on the internal carbon atoms tends towards zero in cations. Vibrational frequencies and infrared intensities have been calculated for the optimized structures of PAH neutrals and cations. The drastic intensity alterations occurring upon ionization are discussed and related to specific changes occurring in the charge distribution. The $C-H$ stretch intensity depends on the partial charge on peripheral hydrogen atoms and reduces in cations as hydrogen atoms become more positive. Pericondensed PAHs show better matching with the observed interstellar infrared bands. The co-added model spectra show profiles similar to the observed astrophysical bands.

*Key words:* PAH; IR Spectra; Aromatic Infrared Bands; Interstellar Molecules; DFT; Charge distribution.

## 1 Introduction

The spectra from diverse astrophysical objects such as HII regions, planetary nebulae, reflection nebulae, post AGB stars, star forming regions, interstellar medium (ISM) of our galaxy and that of outer galaxies show the presence of Aromatic Infrared Bands (AIBs) centred at 3.3, 6.2, 7.7, 8.6, 11.2 and 12.7 $\mu m$ (3030, 1610, 1300, 1160, 890 and 785 $cm^{-1}$) [1–4] with intensity and band profile variations from source to source [4–7]. These bands are spectral signatures attributed to Polycyclic Aromatic Hydrocarbon (PAH) molecules [8–11]. The ubiquitous presence of AIBs makes PAHs important component of the molecular universe and are also considered as possible contributors to the UV extinction curve [12,13] and the diffuse interstellar bands (DIBs) [14–16].

PAHs have planar structure of fused benzenoid rings with the $\pi$ electrons de-localized over the whole carbon skeleton providing high photo-stability and a large surface area for efficient absorption of background radiations. Absorption of a single UV photon results in vibrational heating of the PAH up to temperatures of nearly 1000 K. The isolated molecule de-excites through infrared emissions [10,11]. For a better understanding and identification of the carriers of interstellar AIB features, a widespread effort is being put to measure and calculate the vibrational properties of PAHs [5,17–33]. Strong UV radiations from background stars may also result in ionization of PAHs which complicates the analysis of the resulting composite spectra. The band positions for ionized PAHs differ little from neutrals but there is a remarkable difference in the intensity patterns [20–29].

* Corresponding author
*Email address:* shantanu_r@hotmail.com (Shantanu Rastogi).

The understanding of the IR spectra of PAHs and its variations with size and ionization state is needed to analyse the AIB features from various astrophysical environments. With this view and in continuation of the earlier report on catacondensed PAHs [23], we present here study of some pericondensed PAHs. Pericondensed PAHs are more compact and stable compared to linear PAHs. Studies related to photo-physical stability of PAHs in harsh environments have concluded that PAHs in the ISM must have 50 or more carbon atoms [34–38]. Such large species survive mostly in compact pericondensed forms.

Theoretical ab-initio and normal mode calculations [21–30] have been highly useful in measurement and specific assignment of various experimental features of the PAH spectra. In the present work ten pericondensed PAHs, ranging from four ringed to ten ringed structures (Fig. 1), are studied. Charge distribution and vibrational spectra have been calculated for these PAHs and their cations. The effect of ionization on the charge distribution and its relation to the significant changes occurring in the IR spectra of these PAHs is discussed. astrophysical implications of the results are presented.

## 2 Calculations

Bond lengths, charge distributions and vibrational spectra in absorption are presented to understand the cumulative effect of ionization on pericondensed PAHs. Density Functional Theory (DFT) is employed in the computations using the GAMESS [39] ab-initio program. Optimized geometries, vibrational frequencies and IR intensities are computed for both neutrals and cations using the B3LYP functional in conjunction with a 4-31G basis expansion. The B3LYP approach is computationally economical and for cations gives better

results as compared to SCF or MP2 calculations [40]. Computations with the use of 4-31G basis set are well established [21–23] and need a single scale factor to bring the vibrational frequencies in conjunction with the experimental data [21,23,40] but results in an overestimation of the $C-H$ stretch intensity in the case of neutral molecules. The use of larger basis sets 6-31G or 6-31G**, give comparatively better $C-H$ stretch intensity match with experiments [21,23,40], but computational time increases many–folds and the scaling procedure also gets complicated [41,42]. Therefore, the use of larger basis sets is avoided.

Mulliken population analysis, which is based on wave-function partitioning in terms of basis functions, is used to study the charge distribution. The method is most useful for comparing trends in electron distributions when small or medium sized basis sets are used [43]. The anylysis is thus useful in the study of variations from neutrals to cations.

The calculated frequencies for some smaller PAHs – naphthalene, anthracene and pyrene, were compared with the reported matrix isolation spectra to obtain the best fit scale factor of 0.956. The calculated frequencies of all studied PAHs [23] are scaled by this factor and a good correlation with the reported experimental data, wherever available, is obtained. The calculated spectra have been plotted considering Gaussian profiles with Full Width Half Maximum to be 30 $cm^{-1}$, which is the typical width for PAHs emitting in conditions present in the ISM [10].

## 3 Results

The spectra of PAH cations are remarkably different from their neutral counterparts in terms of intensities of major peaks [5,17–33]. The spectra of neutrals is dominated by $C-H$ stretch and $C-H$ out of plane bend modes, whereas in cations the intensity of $C-H$ in plane bend and $C-C$ stretch modes (1150 – 1600 $cm^{-1}$) are increased by an order of magnitude and the $C-H$ stretch mode intensity is drastically reduced by a similar factor. The $C-H$ out of plane bend mode remains unaffected and has similar intensity in both neutrals and cations. The variations in intensities are attributed to the changes occurring in the charge distribution upon ionization of the molecules as in the case of catacondensed PAHs [23]. In order to pinpoint these changes and to relate them to the variations in the infrared intensities, the charge distribution of studied pericondensed PAHs is presented in Table 1; wherein comparisons for neutrals and cations are shown only for atoms where there is significant change.

Ionization induces small changes as far as the structure of the molecule is concerned with no or little change in bond lengths. To gain insight into structural changes induced by ionization, bond lengths for bonds showing large change are also presented in Table 1. The symmetry of the molecules is preserved in the ionized species except for highly symmetric molecules viz. triphenylene ($D_{3h}$) and coronene($D_{6h}$), which show reduced symmetry upon ionization. It seems that, as a consequence of Jahn-Teller effect [44], upon ionization of such highly symmetric species the $\pi$ orbitals mix to localize on one side of the molecules resulting in reduction of symmetry [45].

The vibrational frequencies and IR intensities are calculated for the optimized geometry of PAHs. The calculated spectra show good match with available experimental and theoretical data wherever present. Vibrational frequencies and intensities of benzo(e)pyrene, anthanthrene, bisanthene, perinaphthacenonaphthacene ($C_{28}H_{14}$) and 2,3,8,9-dibenzo coronene ($C_{30}H_{14}$) are given in Tables 2, 3, 4, 5 and 6 respectively. The results for these molecules are being presented for the first time at this level of calculations. To save space complete vibrational data for all molecules is not being given but may be obtained from the authors upon request.

In *pyrene*, on ionization the major bond length changes are in outer bonds $e, c$ and $b$. Bond $a$, an outer bond shows the minimum change. Maximum change in charge is present in $C2$, an outer carbon. Internal carbon $C5$ is slightly negatively charged in the neutral molecule and becomes nearly zero in cation. In the spectra of pyrene, Fig. 2, two peaks at 850 and 3080 $cm^{-1}$ are respectively due to $C-H$ out of plane bend modes and $C-H$ stretch modes. The peak at 850 $cm^{-1}$ has contributions from both the duo and trio hydrogen atoms. Spectra of the cation shows enhancements in the intensities of modes between 1200 – 1550 $cm^{-1}$, with the $C-C$ stretch mode at 1526.4 $cm^{-1}$ having highest intensity. Two peaks for the $C-H$ out of plane bend mode are present at 684 and 865 $cm^{-1}$. The former is due to the trio set of hydrogen atoms while the latter results from out of plane vibrations of the duo hydrogens.

*Triphenylene* upon ionization looses its symmetry from $D_{3h}$ in neutral to $C_{2v}$ in the cation. The bonds $d$ and $f$ and $e$ and $l$, which were equivalent in the neutral molecule are different in the cation. On ionization, bond $f$ has increased while $l$ has decreased. Significant change is observed in the outer

Table 1
Bond length and charge distribution of studied PAHs

Pyrene

| Bond Lengths | | | Charge Distribution | | |
|---|---|---|---|---|---|
| Bonds* | Neutral | Cation | Atoms* | Neutral | Cation |
| b | 1.403 | 1.423 | C1 | -0.122 | -0.114 |
| c | 1.437 | 1.417 | C2 | -0.159 | -0.101 |
| e | 1.360 | 1.384 | C4 | -0.138 | -0.113 |
| f | 1.427 | 1.417 | H6 | 0.127 | 0.191 |
| | | | H7 | 0.127 | 0.192 |
| | | | H8 | 0.128 | 0.189 |

Triphenylene

| Bond Lengths | | | Charge Distribution | | |
|---|---|---|---|---|---|
| Bonds* | Neutral | Cation | Atoms* | Neutral | Cation |
| f | 1.423 | 1.453 | C1 | -0.123 | -0.101 |
| k | 1.413 | 1.433 | C2 | -0.144 | -0.119 |
| l | 1.465 | 1.428 | C4 | 0.008 | 0.043 |
| | | | C7 | -0.123 | -0.087 |
| | | | C9 | -0.144 | -0.107 |
| | | | H10 | 0.127 | 0.184 |
| | | | H11 | 0.132 | 0.176 |
| | | | H12 | 0.132 | 0.176 |
| | | | H13 | 0.127 | 0.191 |
| | | | H14 | 0.127 | 0.187 |
| | | | H15 | 0.132 | 0.179 |

Perylene

| Bond Lengths | | | Charge Distribution | | |
|---|---|---|---|---|---|
| Bonds* | Neutral | Cation | Atoms* | Neutral | Cation |
| a | 1.374 | 1.387 | C1 | -0.139 | -0.104 |
| c | 1.405 | 1.392 | C2 | -0.125 | -0.114 |
| e | 1.391 | 1.412 | C3 | -0.155 | -0.111 |
| f | 1.475 | 1.451 | H7 | 0.128 | 0.184 |
| | | | H8 | 0.128 | 0.183 |
| | | | H9 | 0.130 | 0.175 |

Table 1 contd ...

Benzo(e)pyrene

| Bond Lengths | | | Charge Distribution | | |
|---|---|---|---|---|---|
| Bonds* | Neutral | Cation | Atoms* | Neutral | Cation |
| d | 1.424 | 1.445 | C1 | -0.123 | -0.114 |
| e | 1.467 | 1.448 | C2 | -0.149 | -0.098 |
| f | 1.402 | 1.421 | C4 | 0.013 | 0.029 |
| l | 1.434 | 1.414 | C5 | -0.144 | -0.129 |
| m | 1.358 | 1.381 | C6 | -0.123 | -0.105 |
| n | 1.404 | 1.421 | C7 | -0.151 | -0.100 |
| | | | C9 | -0.139 | -0.117 |
| | | | H11 | 0.127 | 0.185 |
| | | | H12 | 0.131 | 0.183 |
| | | | H13 | 0.132 | 0.166 |
| | | | H14 | 0.127 | 0.178 |
| | | | H15 | 0.127 | 0.186 |
| | | | H16 | 0.129 | 0.187 |

Anthanthrene

| Bond Lengths | | | Charge Distribution | | |
|---|---|---|---|---|---|
| Bonds* | Neutral | Cation | Atoms* | Neutral | Cation |
| c | 1.396 | 1.415 | C1 | -0.151 | -0.113 |
| e | 1.442 | 1.429 | C3 | -0.164 | -0.116 |
| f | 1.357 | 1.370 | C5 | -0.135 | -0.117 |
| g | 1.443 | 1.429 | C6 | -0.135 | -0.118 |
| i | 1.384 | 1.405 | C8 | -0.198 | -0.144 |
| | | | H12 | 0.127 | 0.179 |
| | | | H13 | 0.128 | 0.181 |
| | | | H14 | 0.127 | 0.181 |
| | | | H15 | 0.129 | 0.177 |
| | | | H16 | 0.129 | 0.176 |
| | | | H17 | 0.128 | 0.181 |

bond $k$ and inner bond $f$. Large change in charge as a result of ionization is for the outer carbon $C7$ while significant changes are there in outer carbons $C9, C2, C1$ and the inner carbon $C4$. Charges on carbons $C3$ and $C5$ are negligible in both neutral and ionized species. The spectra of neutral, shown

Table 1 contd ...

| Coronene | | | | | |
|---|---|---|---|---|---|
| Bond Lengths | | | Charge Distribution | | |
| Bonds* | Neutral | Cation | Atoms* | Neutral | Cation |
| b | 1.423 | 1.435 | C1 | -0.145 | -0.134 |
| c | 1.371 | 1.394 | C2 | -0.145 | -0.108 |
| d | 1.423 | 1.406 | C3 | -0.145 | -0.126 |
| f | 1.423 | 1.440 | C5 | 0.047 | 0.074 |
| | | | H8 | 0.129 | 0.176 |
| | | | H9 | 0.129 | 0.179 |
| | | | H10 | 0.129 | 0.181 |
| Bisanthene | | | | | |
| Bond Lengths | | | Charge Distribution | | |
| Bonds* | Neutral | Cation | Atoms* | Neutral | Cation |
| a | 1.371 | 1.381 | C1 | -0.137 | -0.114 |
| b | 1.409 | 1.399 | C3 | -0.159 | -0.125 |
| c | 1.390 | 1.403 | C6 | -0.192 | -0.144 |
| d | 1.471 | 1.460 | H9 | 0.129 | 0.172 |
| i | 1.438 | 1.428 | H10 | 0.129 | 0.174 |
| j | 1.451 | 1.431 | H11 | 0.131 | 0.168 |
| | | | H12 | 0.129 | 0.176 |

in Fig. 2, is simple consisting mainly of the $C-H$ stretch and out of plane bands. The three sets of quartet hydrogens contribute to the intensity of $C-H$ out of plane bend at 749 $cm^{-1}$. Due to reduced symmetry the spectra of the cation is more complex. Several intense bands are present between the 1000 – 1600 $cm^{-1}$ range. The most intense feature lies at 1356 $cm^{-1}$.

*Perylene* shows similarity with pyrene in terms of bond length and charge distribution changes upon ionization. Major bond length changes are restricted to outer bonds of the molecule. Maximum change in charge is for the carbons $C1$ and $C3$. The inner carbon $C6$ has small charge in neutral and is almost zero in the cation. Spectra of neutral perylene (Fig. 3) has a $C-H$ out of plane bend mode at 815 $cm^{-1}$ with a shoulder at 765.1 $cm^{-1}$. The intensity evolves

Table 1 contd ...

$C_{28}H_{14}$

| Bond Lengths | | | Charge Distribution | | |
|---|---|---|---|---|---|
| Bonds* | Neutral | Cation | Atoms* | Neutral | Cation |
| a | 1.444 | 1.435 | C1 | -0.135 | -0.124 |
| b | 1.382 | 1.397 | C3 | -0.198 | -0.161 |
| c | 1.423 | 1.412 | C4 | 0.089 | 0.076 |
| d | 1.398 | 1.408 | C5 | -0.193 | -0.144 |
| g | 1.380 | 1.388 | C7 | -0.144 | -0.116 |
| h | 1.408 | 1.400 | C9 | -0.167 | -0.127 |
| i | 1.393 | 1.407 | C10 | 0.049 | 0.037 |
| j | 1.445 | 1.436 | C11 | -0.132 | -0.116 |
| l | 1.433 | 1.423 | H15 | 0.129 | 0.166 |
| m | 1.446 | 1.437 | H16 | 0.129 | 0.171 |
| | | | H17 | 0.129 | 0.175 |
| | | | H18 | 0.128 | 0.171 |
| | | | H19 | 0.128 | 0.175 |
| | | | H20 | 0.127 | 0.174 |
| | | | H21 | 0.129 | 0.169 |

from the in phase out of plane vibrations of all the trio hydrogen atoms. The perylene cation spectra has two similar peaks for the $C-H$ out of plane bend mode as in neutral, present at 814 and 743 $cm^{-1}$. Two peaks of almost equal intensity are present at 1292 and 1310 $cm^{-1}$. The most intense peak of the cation spectra is $C-C$ stretch mode at 1525 $cm^{-1}$.

Ionization of *benzo(e)pyrene* produces major bond length changes in the outer bonds $e, f, l, m$ and $n$ and the inner bond $d$. Maximum change in the charge upon ionization is for the carbon atoms $C2$ and $C7$ while significant change is there in $C6, C9$ and $C10$ atoms. Internal carbon $C10$ has zero charge in the cation. The calculated vibrational data compares well with the reported experimental data for both neutral and cation (Table 2). Two trio and one quartet group of hydrogens contribute to the most intense peak at 752 $cm^{-1}$,

Table 1 contd ...

$C_{30}H_{14}$

| Bond Lengths | | | Charge Distribution | | |
|---|---|---|---|---|---|
| Bonds* | Neutral | Cation | Atoms* | Neutral | Cation |
| b | 1.408 | 1.416 | C1 | -0.157 | -0.119 |
| c | 1.424 | 1.413 | C4 | -0.199 | -0.161 |
| d | 1.380 | 1.395 | C6 | -0.135 | -0.122 |
| k | 1.446 | 1.436 | H10 | 0.128 | 0.174 |
| | | | H11 | 0.128 | 0.174 |
| | | | H12 | 0.129 | 0.172 |
| | | | H13 | 0.131 | 0.167 |

Ovalene

| Bond Lengths | | | Charge Distribution | | |
|---|---|---|---|---|---|
| Bonds* | Neutral | Cation | Atoms* | Neutral | Cation |
| a | 1.364 | 1.375 | C1 | -0.139 | -0.119 |
| b | 1.432 | 1.420 | C2 | -0.142 | -0.133 |
| c | 1.414 | 1.427 | C4 | -0.151 | -0.127 |
| d | 1.379 | 1.370 | C5 | 0.073 | 0.060 |
| e | 1.434 | 1.426 | C6 | -0.204 | -0.153 |
| l | 1.435 | 1.423 | H10 | 0.129 | 0.170 |
| | | | H11 | 0.129 | 0.170 |
| | | | H12 | 0.129 | 0.169 |
| | | | H13 | 0.129 | 0.175 |

*For Bond labeling and atom numbering refer to Fig. 1.

while the peak at 833.8 $cm^{-1}$ is due to the duo hydrogens in the spectra of neutral benzo(e)pyrene (Fig. 3). Because of lower symmetry of this molecule, the $C-H$ stretch mode intensity is divided amongst several moderate peaks, which seem to merge in the plot using FWHM of 30 $cm^{-1}$. Spectra of cation shows similar $C-H$ out of plane bend features as in the neutral species. The most intense feature at 1300 $cm^{-1}$ is an overlap of neighbouring three $C-C$ stretch modes.

Ionization of *anthanthrene* results in bond length changes of $c, e, f, g$ and $i$ bonds. Change in the charges is mainly for carbons $C8, C3$ and $C1$. The inter-

Table 2
Comparison of IR Frequencies ($cm^{-1}$) and Relative Intensities for benzo(e)pyrene*

| Neutral | | | | | Cation | | | |
|---|---|---|---|---|---|---|---|---|
| Computed Result | | | Experimental Result[1] | | Computed Result | | Experimental Result[2] | |
| | Freq ($cm^{-1}$) | Rel. Int. | Freq ($cm^{-1}$) | Rel. Int. | | Freq ($cm^{-1}$) | Rel. Int. | Freq ($cm^{-1}$) | Rel. Int. |
| $B_2$ | 549.8 | 0.05 | 554.5 | 0.05 | $B_2$ | 628.8 | 0.06 | | |
| $B_1$ | 567.6 | 0.06 | 570.6 | 0.07 | $B_1$ | 676.1 | 0.11 | 685.7 | 0.15 |
| $B_2$ | 634.8 | 0.03 | 645.9 | 0.02 | $A_2$ | 692.7 | 0.06 | | |
| $B_1$ | 701.9 | 0.09 | 711.8 | 0.18 | $A_2$ | 751.1 | 0.09 | | |
| $B_1$ | 752.7 | 1.00 | 750.0 | 1.00 | $B_1$ | 760.1 | 0.47 | | |
| | | | 771.1 | 0.15 | $B_1$ | 852.9 | 0.25 | 848.0 | 0.22 |
| $B_1$ | 833.8 | 0.67 | 830.1 | 0.51 | $B_2$ | 861.9 | 0.11 | 873.3 | 0.13 |
| | | | 842.9 | 0.14 | $A_2$ | 935.4 | 0.06 | | |
| $B_1$ | 896.5 | 0.09 | 898.2 | 0.03 | $A_2$ | 978.5 | 0.13 | | |
| $B_2$ | 1033.6 | 0.03 | 1037.8 | 0.04 | $B_2$ | 1166.0 | 0.05 | | |
| $A_2$ | 1110.1 | 0.03 | 1106.9 | 0.04 | $A_2$ | 1206.9 | 0.34 | 1193.9 | 0.21 |
| $B_2$ | 1207.4 | 0.04 | 1191.8 | 0.09 | $B_2$ | 1215.9 | 0.08 | | |
| $A_2$ | 1311.6 | 0.05 | 1320.6 | 0.07 | $A_2$ | 1272.1 | 0.27 | 1264.3 | 0.14 |
| $B_2$ | 1317.2 | 0.04 | | | $A_2$ | 1294.3 | 0.43 | 1308.2 | 0.19 |
| $A_2$ | 1399.3 | 0.15 | 1413.5 | 0.20 | $B_2$ | 1299.1 | 0.78 | | |
| $B_2$ | 1432.5 | 0.09 | 1444.1 | 0.19 | $B_2$ | 1319.2 | 0.47 | 1336.0 | 0.81 |
| $B_2$ | 1460.9 | 0.17 | 1478.9 | 0.08 | | | | 1349.2 | 1.00 |
| $B_2$ | 1504.7 | 0.07 | | | $B_2$ | 1335.6 | 0.16 | 1357.0 | 0.15 |
| $A_2$ | 1584.9 | 0.15 | 1593.2 | 0.03 | $A_2$ | 1338.9 | 0.07 | | |
| $A_2$ | 3031.5 | 0.05 | 3018.0 | \| | $B_2$ | 1386.0 | 0.17 | 1368.2 | 0.13 |
| $B_2$ | 3049.8 | 0.41 | 3036.0 | \| | $A_2$ | 1405.8 | 0.15 | 1410.5 | 0.41 |
| $B_2$ | 3051.9 | 0.13 | 3059.7 | 1.23 | $B_2$ | 1430.9 | 0.12 | 1435.6 | 0.09 |
| $B_2$ | 3064.5 | 0.32 | | \| | $B_2$ | 1526.2 | 1.00 | 1556.8 | 0.88 |
| $A_2$ | 3067.8 | 0.23 | | \| | $B_2$ | 1538.4 | 0.08 | | |
| $B_2$ | 3068.3 | 0.35 | | \| | $A_2$ | 1540.5 | 0.07 | | |
| $A_2$ | 3085.1 | 0.46 | | \| | $B_2$ | 1579.2 | 0.14 | | |
| $A_2$ | 3103.1 | 0.48 | 3091.0 | \| | $B_2$ | 3073.2 | 0.04 | | |
| $B_2$ | 3105.9 | 0.13 | 3108.7 | \| | $A_2$ | 3122.4 | 0.06 | | |

Max. absolute int. Neutral - 2.32 Debye$^2$/AMU-Å$^2$; Cation - 5.42 Debye$^2$/AMU-Å$^2$
* Irreducible representations are given for each normal mode.
[1] Ref. 31
[2] Ref. 32

nal carbon atoms $C10$ and $C11$ have very small charge in neutral which becomes nearly zero in the cation. Theoretical vibrational data for anthanthrene is given in Table 3 and the spectra are shown in Fig. 4. Three distinct peaks for the $C-H$ out of plane bend modes are present at 752, 807 and 887 $cm^{-1}$. The 752 $cm^{-1}$ peak reflects the motion of the trio hydrogen atoms while the mode at 807 $cm^{-1}$ is a mix of out of plane vibrations of duo and trio hydrogen atoms. 887 $cm^{-1}$ mode corresponds to the out of plane vibrations of solo hydrogen atoms and is of highest intensity. The spectrum of the cation has similar $C-H$ out of plane bend features as in neutral but more intense peaks are present in the 1200 – 1600 $cm^{-1}$ range, which is complex and has strong modes at 1242 and 1563 $cm^{-1}$.

*Coronene* is a highly symmetric pericondensed PAH with $D_{6h}$ point group symmetry in neutral species. Ionization results in a reduced symmetry ($D_{2h}$) though the structure of the molecules is not much changed. Upon ionization, major bond length changes are present in bonds $c, d$ and $f$, where $f$ is one of the inner $C-C$ bonds. Charges of $C2, C3$ and $C5$ show maximum changes while charge of carbon $C4$ remains unchanged. Charge on internal carbons $C6$ and $C7$ is almost zero in both neutral and cation. Fig. 4 shows the spectra of coronene neutral and cation. In neutral the out of plane motion of the duo hydrogens contribute to 867 $cm^{-1}$ peak. The cation spectra is rich in intense features between the range 1200 – 1550 $cm^{-1}$ with the most intense one at 1536 $cm^{-1}$. Matrix isolation spectroscopy of coronene cation [32] show the most intense feature for the $C-H$ out of plane bend mode. This seems to be the contribution from neutral contaminants. Gas phase study on coronene cation [46] correlates better with the present theoretical spectra.

Upon ionization of *bisanthene*, maximum change in bond length is in the inner

Table 3
Comparison of IR Frequencies ($cm^{-1}$) and Relative Intensities for anthanthrene*

| Neutral | | | | | Cation[1] | | |
|---|---|---|---|---|---|---|---|
| Computed Result | | | Experimental Result[2] | | Computed Result | | |
| | Freq ($cm^{-1}$) | Rel. Int. | Freq ($cm^{-1}$) | Rel. Int. | | Freq ($cm^{-1}$) | Rel. Int. |
| $A_u$ | 180.5 | 0.06 | | | $A_u$ | 174.6 | 0.04 |
| $B_u$ | 457.9 | 0.05 | | | $A_u$ | 679.0 | 0.07 |
| $A_u$ | 686.1 | 0.11 | 688.7 | 0.37 | $A_u$ | 743.9 | 0.14 |
| $A_u$ | 752.7 | 0.45 | 752.4 | 0.60 | $A_u$ | 822.4 | 0.23 |
| $A_u$ | 807.8 | 0.42 | 809.1 | 0.42 | $A_u$ | 908.9 | 0.34 |
| $A_u$ | 887.9 | 0.94 | 877.2 | 0.75 | $B_u$ | 1155.9 | 0.05 |
| $A_u$ | 900.7 | 0.13 | 895.3 | 0.15 | $B_u$ | 1189.1 | 0.06 |
| $B_u$ | 1073.8 | 0.06 | | | $B_u$ | 1196.8 | 0.05 |
| $B_u$ | 1187.7 | 0.08 | 1169.6 | 0.09 | $B_u$ | 1242.8 | 0.84 |
| $B_u$ | 1319.7 | 0.07 | 1317.5 | 0.02 | $B_u$ | 1269.3 | 0.25 |
| $B_u$ | 1428.8 | 0.14 | | | $B_u$ | 1329.3 | 0.14 |
| $B_u$ | 1543.5 | 0.11 | 1547.9 | 0.03 | $B_u$ | 1339.4 | 0.13 |
| $B_u$ | 1581.2 | 0.11 | 1597.4 | 0.03 | $B_u$ | 1352.6 | 0.33 |
| $B_u$ | 1608.9 | 0.09 | 1628.7 | 0.07 | $B_u$ | 1438.8 | 0.11 |
| $B_u$ | 3017.1 | 0.09 | | | $B_u$ | 1443.8 | 0.11 |
| $B_u$ | 3019.2 | 0.25 | | | $B_u$ | 1479.2 | 0.10 |
| $B_u$ | 3027.1 | 0.17 | | | $B_u$ | 1512.9 | 0.08 |
| $B_u$ | 3039.4 | 0.75 | | | $B_u$ | 1545.4 | 0.06 |
| $B_u$ | 3044.9 | 1.00 | | | $B_u$ | 1562.9 | 1.00 |
| $B_u$ | 3067.1 | 0.81 | | | $B_u$ | 3061.8 | 0.07 |

Max. absolute int. Neutral - 2.21 Debye$^2$/AMU-Å$^2$; Cation - 5.84 Debye$^2$/AMU-Å$^2$
* Irreducible representations are given for each normal mode.
[1] No experimental data available for cation.
[2] Condensed phase IR data, NIST Chemistry Web Book (http://webbook.nist.gov/chemistry).

most bond $j$. Outer bonds $a, b, c$ and $d$ also show significant change. Charges of outer carbons $C6, C3$ and $C1$ shows large change while $C7$ an inner carbon also shows significant change. The charge of carbons $C7$ and $C8$ tends towards zero in cation. The calculated frequencies and intensities are presented in Table 4. To the best of our knowledge no experimental spectra is reported for this

PAH. The spectrum of neutral bisanthene (Fig. 5) is similar to other PAHs but has an exceptionally intense feature at 1596 $cm^{-1}$. This feature involves stretching of the outer $C-C$ bonds in the bay region (bonds $c$ and $d$). The intense $C-C$ stretch modes present in the spectrum of the cation involve other outer carbons and bonds as well and the modes are different from the one present in the neutral. Similar feature is also present in the spectra of perylene having a similar bay structure. The feature at 757 and 876 $cm^{-1}$ are respectively due to trio and solo hydrogen atoms. The cation spectra is also different from the spectra of other PAH cations. The feature at 1283 $cm^{-1}$ is the most intense while all other modes have relatively smaller intensity unlike other PAH cations.

Bond length changes in *peri-naphthacenonaphthacene* ($C_{28}H_{14}$) with ionization are small and mainly restricted to outer bonds. Maximum change is for bonds $b$ and $i$ while inner bonds $o$, $p$ and $q$ show negligible changes. Internal carbons 12, 13 and 14 have very small charge in the neutral as well as in the cation. The maximum change in charge is for $C5$. The neutral molecule has a simple spectrum (Fig. 5) with a high intensity $C-H$ stretch peak at 3053 $cm^{-1}$ and an intense peak at 887 $cm^{-1}$ due to out of plane bend vibrations of solo hydrogens. Calculated intensities and frequencies for $C_{28}H_{14}$ neutral and cation have been presented in Table 5. The $C_{28}H_{14}$ cation spectrum has three intense peaks at 1223 ($C-H$ in plane bending), 1348 and 1592 $cm^{-1}$ (mainly $C-C$ stretch combined with $C-H$ in plane vibrations).

Upon ionization, *2,3,8,9-dibenzo coronene* ($C_{30}H_{14}$), experiences bond length changes in outer bonds. Maximun change in bond is for the outer bond $d$. Insignificant change is there in inner bond $i$. Charge changes are for outer carbon atoms and the inner ones are nearly neutral in both the neutral and

Table 4
Computed IR Frequencies ($cm^{-1}$) and Relative Intensities for bisanthene[1*]

| Neutral | | | Cation | | |
|---|---|---|---|---|---|
| | Freq ($cm^{-1}$) | Rel. Int. | | Freq ($cm^{-1}$) | Rel. Int. |
| $B_{2u}$ | 303.1 | 0.08 | $B_{3u}$ | 92.6 | 0.02 |
| $B_{3u}$ | 537.3 | 0.08 | $B_{2u}$ | 300.6 | 0.04 |
| $B_{2u}$ | 644.9 | 0.12 | $B_{3u}$ | 528.5 | 0.04 |
| $B_{3u}$ | 757.8 | 0.97 | $B_{2u}$ | 646.8 | 0.04 |
| $B_{3u}$ | 761.3 | 0.09 | $B_{3u}$ | 755.5 | 0.18 |
| $B_{3u}$ | 776.9 | 0.28 | $B_{3u}$ | 785.7 | 0.28 |
| $B_{3u}$ | 876.9 | 0.73 | $B_{3u}$ | 900.2 | 0.15 |
| $B_{2u}$ | 905.4 | 0.12 | $B_{3u}$ | 943.6 | 0.05 |
| $B_{3u}$ | 911.4 | 0.16 | $B_{1u}$ | 1209.2 | 0.25 |
| $B_{1u}$ | 1091.1 | 0.05 | $B_{2u}$ | 1261.3 | 0.07 |
| $B_{2u}$ | 1232.9 | 0.06 | $B_{1u}$ | 1283.1 | 1.00 |
| $B_{2u}$ | 1265.4 | 0.24 | $B_{1u}$ | 1300.9 | 0.12 |
| $B_{2u}$ | 1290.7 | 0.06 | $B_{2u}$ | 1328.9 | 0.06 |
| $B_{1u}$ | 1326.5 | 0.08 | $B_{2u}$ | 1456.6 | 0.16 |
| $B_{1u}$ | 1347.2 | 0.06 | $B_{1u}$ | 1470.4 | 0.05 |
| $B_{2u}$ | 1450.2 | 0.12 | $B_{2u}$ | 1524.7 | 0.09 |
| $B_{2u}$ | 1470.2 | 0.05 | $B_{1u}$ | 1548.3 | 0.16 |
| $B_{1u}$ | 1593.4 | 0.16 | $B_{2u}$ | 1571.8 | 0.11 |
| $B_{2u}$ | 1596.1 | 0.43 | $B_{2u}$ | 3059.3 | 0.06 |
| $B_{2u}$ | 3020.6 | 0.27 | $B_{1u}$ | 3094.2 | 0.11 |
| $B_{2u}$ | 3033.1 | 0.46 | | | |
| $B_{1u}$ | 3034.8 | 0.39 | | | |
| $B_{2u}$ | 3060.5 | 0.18 | | | |
| $B_{2u}$ | 3072.1 | 0.92 | | | |
| $B_{1u}$ | 3078.1 | 1.00 | | | |

Max. absolute int. Neutral - 2.45 Debye$^2$/AMU-Å$^2$; Cation - 7.89 Debye$^2$/AMU-Å$^2$
[1] No experimental data available.
* Irreducible representations are given for each normal mode.

cationic species. Significant charge changes are for $C1$ and $C4$. The spectrum of the neutral molecule (Fig. 6) consists of two peaks at 905 and 759 $cm^{-1}$ for out of plane vibrations of hydrogen atoms. The $C-H$ stretch vibrations produce

Table 5
Computed IR Frequencies ($cm^{-1}$) and Relative Intensities for $C_{28}H_{14}$[1*]

| Neutral | | | Cation | | |
|---|---|---|---|---|---|
| | Freq ($cm^{-1}$) | Rel. Int. | | Freq ($cm^{-1}$) | Rel. Int. |
| $A_u$ | 182.6 | 0.03 | $A_u$ | 680.3 | 0.08 |
| $B_u$ | 472.1 | 0.03 | $A_u$ | 756.3 | 0.04 |
| $B_u$ | 586.4 | 0.04 | $A_u$ | 823.5 | 0.14 |
| $A_u$ | 682.7 | 0.16 | $A_u$ | 912.9 | 0.18 |
| $A_u$ | 743.9 | 0.09 | $B_u$ | 1134.7 | 0.03 |
| $A_u$ | 779.4 | 0.12 | $B_u$ | 1160.0 | 0.03 |
| $A_u$ | 809.9 | 0.25 | $B_u$ | 1175.9 | 0.07 |
| $A_u$ | 886.8 | 0.57 | $B_u$ | 1195.1 | 0.06 |
| $A_u$ | 893.4 | 0.15 | $B_u$ | 1223.2 | 0.34 |
| $B_u$ | 1057.7 | 0.04 | $B_u$ | 1348.4 | 1.00 |
| $B_u$ | 1124.8 | 0.03 | $B_u$ | 1395.3 | 0.15 |
| $B_u$ | 1186.5 | 0.04 | $B_u$ | 1437.2 | 0.03 |
| $B_u$ | 1227.9 | 0.05 | $B_u$ | 1465.7 | 0.09 |
| $B_u$ | 1307.1 | 0.03 | $B_u$ | 1535.2 | 0.06 |
| $B_u$ | 1411.1 | 0.04 | $B_u$ | 1592.4 | 0.66 |
| $B_u$ | 1416.1 | 0.04 | $B_u$ | 3067.7 | 0.04 |
| $B_u$ | 1438.3 | 0.10 | $B_u$ | 3074.9 | 0.08 |
| $B_u$ | 1483.9 | 0.04 | | | |
| $B_u$ | 1553.4 | 0.04 | | | |
| $B_u$ | 1563.3 | 0.08 | | | |
| $B_u$ | 1619.3 | 0.07 | | | |
| $B_u$ | 3018.0 | 0.09 | | | |
| $B_u$ | 3021.4 | 0.21 | | | |
| $B_u$ | 3025.9 | 0.06 | | | |
| $B_u$ | 3035.5 | 0.18 | | | |
| $B_u$ | 3046.1 | 0.54 | | | |
| $B_u$ | 3053.4 | 1.00 | | | |

Max. absolute int. Neutral - 3.97 Debye$^2$/AMU-Å$^2$; Cation - 11.75 Debye$^2$/AMU-Å$^2$
[1] No experimental data available.
* Irreducible representations are given for each normal mode.

Table 6
Computed IR Frequencies ($cm^{-1}$) and Relative Intensities for $C_{30}H_{14}$[1*]

| Neutral | | | Cation | | |
|---|---|---|---|---|---|
| | Freq ($cm^{-1}$) | Rel. Int. | | Freq ($cm^{-1}$) | Rel. Int. |
| $B_{1u}$ | 388.1 | 0.04 | $B_{1u}$ | 388.8 | 0.03 |
| $B_{3u}$ | 503.2 | 0.15 | $B_{3u}$ | 533.9 | 0.11 |
| $B_{3u}$ | 537.4 | 0.08 | $B_{3u}$ | 756.1 | 0.25 |
| $B_{1u}$ | 710.4 | 0.04 | $B_{3u}$ | 792.7 | 0.17 |
| $B_{3u}$ | 758.5 | 0.41 | $B_{3u}$ | 924.4 | 0.63 |
| $B_{3u}$ | 785.4 | 0.07 | $B_{2u}$ | 1030.9 | 0.04 |
| $B_{3u}$ | 904.8 | 0.90 | $B_{2u}$ | 1171.1 | 0.04 |
| $B_{3u}$ | 975.8 | 0.04 | $B_{2u}$ | 1194.3 | 0.05 |
| $B_{2u}$ | 1198.3 | 0.04 | $B_{2u}$ | 1205.2 | 0.04 |
| $B_{1u}$ | 1256.7 | 0.08 | $B_{1u}$ | 1245.4 | 0.43 |
| $B_{2u}$ | 1274.4 | 0.07 | $B_{2u}$ | 1247.3 | 0.42 |
| $B_{1u}$ | 1380.8 | 0.07 | $B_{2u}$ | 1287.9 | 0.23 |
| $B_{1u}$ | 1463.9 | 0.07 | $B_{2u}$ | 1326.5 | 0.65 |
| $B_{2u}$ | 1552.2 | 0.06 | $B_{2u}$ | 1374.5 | 0.04 |
| $B_{1u}$ | 1556.9 | 0.22 | $B_{1u}$ | 1387.7 | 0.07 |
| $B_{1u}$ | 1599.8 | 0.04 | $B_{1u}$ | 1457.1 | 0.05 |
| $B_{2u}$ | 1602.3 | 0.02 | $B_{2u}$ | 1462.6 | 0.18 |
| $B_{2u}$ | 3050.0 | 0.31 | $B_{1u}$ | 1486.5 | 0.07 |
| $B_{2u}$ | 3056.0 | 0.20 | $B_{2u}$ | 1527.1 | 0.66 |
| $B_{2u}$ | 3066.3 | 0.62 | $B_{1u}$ | 1541.1 | 0.05 |
| $B_{1u}$ | 3079.8 | 1.00 | $B_{1u}$ | 1564.9 | 0.05 |
| | | | $B_{2u}$ | 1570.9 | 1.00 |
| | | | $B_{2u}$ | 3086.1 | 0.14 |

Max. absolute int. Neutral - 3.85 Debye$^2$/AMU-Å$^2$; Cation - 4.99 Debye$^2$/AMU-Å$^2$
[1] No experimental data available.
* Irreducible representations are given for each normal mode.

a high intensity peak at 3080 $cm^{-1}$. Ionization results in a more complex spectrum with several moderate intense peaks in 1200–1600 $cm^{-1}$ range. The most intense peak lies at 1571 $cm^{-1}$ corresponding to $C-C$ stretch vibrations. Table 6 gives the calculated frequencies and intensities for neutral and cations.

Ionization of *ovalene* shows relatively small bond length changes compared to other pericondensed PAHs. Major bond length changes are in bonds $a, b, c, e$ and $l$. Charge of carbon $C6$ shows maximum change while significant changes are seen for carbons $C1, C4$ and $C7$. The three internal carbons $C7$, $C8$ and $C9$ in ovalene have nearly zero charge on them in the cation. The spectrum of neutral ovalene has two peaks for $C-H$ out of plane bend vibrations in the 800 – 900 $cm^{-1}$ region at 847 $cm^{-1}$ and 902 $cm^{-1}$ corresponding respectively to the duo and solo hydrogens (Fig. 6). The $C-H$ stretch range consists of a complex blend of several peaks. The 1200 – 1600 $cm^{-1}$ region spectra of ovalene cation has intense peaks at 1246, 1316 and 1557 $cm^{-1}$ along with several moderate intensity features.

In all the PAHs studied the overall effect of ionization on the $C-C$ bond lengths is mostly restricted to the outer bonds while in few cases the inner ones also change. Bisanthene and ovalene on ionization show maximum bond length change in the central inner bond of their structure. The charge distribution of neutral pericondensed PAHs is similar to that of the catacondensed PAHs [23]. The magnitude of charge on all hydrogen atoms is comparable (0.13) in neutral molecules irrespective of the PAH size and peripheral configuration (solo, duo, trio and quartet) of the hydrogen atoms, but the linked carbon atoms have different values of charge. Upon ionization, the charge on all hydrogen atoms increases by almost a similar fraction but the change in charge of the carbons show variations. The internal pericondensed carbon atoms have small negative charge in neutrals and become nearly zero in cations. Major charge changes on ionization occur in the peripheral atoms with few inner atoms also registering significant charge change. The solo carbon atoms, i.e. the carbons bonded with solo hydrogen atom have the maximum negative charge, as in anthanthrene,

bisanthene, $C_{28}H_{14}$, $C_{30}H_{14}$ and ovalene. These carbons also show maximum change in charge with ionization. Due to the varying shapes and structural symmetry of Pericondensed PAHs, the variations with PAH size are not as apparent as in linear polyacenes [23].

## 4 Discussion

The vibrational features of PAHs having different shapes, sizes and charge states present some similarities but show variations in band positions and intensities. A study of these variations can help in the understanding and analysis of the observed AIBs which in turn can put constraints on the type of PAH population and chemistry of the ISM. Studies of PAHs reported earlier [21–23] and the current one show that the band position shifts on ionization are small. This suggests that the effect of ionization on the structure of PAHs is not significant [23,24]. It is the drastic change in band intensities that make the study of PAH ions important. The change in charge distribution upon ionization induces larger or smaller dipole variations for the same vibrational motion. The study of charge distribution can help in understanding and identifying specific variations that affect the IR intensities.

While the spectra of small cations is complex, the spectra of the larger ones is simpler in nature. The three main bands in the spectra of cations between 1100 – 1600 $cm^{-1}$ arise from $C-C$ stretch and $C-H$ in plane vibrations. It is illuminating to identify specific atoms involved in these normal modes. For all studied PAHs the mode around 1200 $cm^{-1}$ has mainly in plane $C-H$ bending vibrations with insignificant vibrations of carbon atoms. The mode near 1300 $cm^{-1}$ is chiefly $C-C$ stretch mode having motion of the outer carbon atoms

and little contribution of inner carbons. In cations of coronene, anthanthrene and $C_{28}H_{14}$ along with outer carbons the inner carbons also have significant contribution towards this mode. In coronene it is the central ring motion, in anthanthrene inner bond $m$ and in $C_{28}H_{14}$ the inner bonds $o$ and $q$ show significant vibrations. The central bonds of ovalene ($l$) and bisanthene ($j$) for this mode show translational motion as seen for the linear catacondensed PAH cations [23]. For the intense band at 1326 $cm^{-1}$ of $C_{30}H_{14}$, the in plane $C-H$ bending of duo and trio hydrogens contribute significantly along with small contribution of inner bond $j$. The 1550 $cm^{-1}$ feature is also mainly due to $C-C$ stretch vibrations of outer atoms. Ovalene has contributions from vibrations within the two inner rings and outer carbons C1 and C2. In $C_{30}H_{14}$ this mode is antisymmetric vibration of the two opposite end bonds $f$. Both the 1300 and 1550 $cm^{-1}$ modes have contributions from $C-H$ in plane vibrations as well and there is no intense pure $C-C$ stretch mode. In most of the cases the change in charge upon ionization is restricted to the outer carbons and these are the ones that contribute significantly to the high intensity modes in cations.

The effect of ionization on the $C-H$ stretch mode intensity is particularly interesting. The intensity of this mode depends on the charge of the hydrogen atoms in the molecule. In $PAH^+$ the positive charge on hydrogen increases and as a result the $C-H$ stretch intensity drastically decreases. This charge effect can be tested by calculating the spectra of negatively-charged PAHs, as shown in Fig. 7. It is clear that the $C-H$ stretch intensity goes on increasing with the addition of electrons. This trend is also seen in naphthalene [23] and other PAHs [22].

The intensity of the $C-H$ stretch mode is also affected by the size of the

PAH cation. As the cation size increases the additional charge is distributed over a larger number of atoms so large cations have lesser charge variation compared to neutrals and hence stronger $C-H$ stretch mode. The absolute intensity for this mode does not show significant increase with increasing size in our case but studies on very large PAH cations (having nearly 100 carbon atoms) [28,47] do show increase in the $C-H$ stretch intensity.

Amongst different $C-H$ out of plane vibrations the intensity corresponding to solo hydrogen atoms (890 $cm^{-1}$), wherever present, is maximum except for bisanthene. Earlier experimental and theoretical studies [48] also point to the fact that in large compact PAHs the solo $C-H$ out of plane mode has higher intensity than other $C-H$ out of plane modes and matches the intense AIB feature at 11.2 $\mu m$. In catacondensed and smaller PAHs [23] this is generally not the highest intensity $C-H$ out of plane mode. The out of plane modes due to different peripheral structure around the rings lead to different peak positions. Therefore the profile of the 11.2 $\mu m$ AIB may be useful in predicting the peripheral structure and ionized state of the emitting molecules [49].

## 5 Astrophysical Implications

The astrophysical infrared emissions depend on the excitation and internal conversion mechanisms in possible PAHs and result from transitions in higher vibrational levels. This may cause the emission features to be broader and slightly red shifted with respect to laboratory absorption bands. Laboratory emission spectra or an emission model [36] is most suitable for direct comparison with AIBs. Obtaining emission spectra in conditions close to interstellar is difficult and only a few studies have been performed [18–20,50]. An alternative

is to use the results of DFT calculations as inputs for emission models [51,52].

The 3.3 $\mu m$, 8.6 $\mu m$ and 11.2 $\mu m$ AIBs arise respectively from the $C-H$ stretch, $C-H$ in plane and $C-H$ out of plane vibrations and the 6.2 $\mu m$ and 7.7 $\mu m$ bands from the $C-C$ skeletal vibrations. Since, all these bands are from the PAH family of molecules, distinct relation should exist between these features. The feature variations depend on the size and charge state of PAHs that reflect the local physical conditions of the ISM. An understanding of the IR spectra of individual PAHs and their cumulative result can lead to the use of AIB observation as an astrophysical probe. Spectra of neutral PAHs only show good position match with the observed spectra while the cations provide a better match for the intensity. More cations seem to be present in star forming regions and regions having a strong UV flux while a mixture of neutrals and cations seems to be the source of AIBs in benign environments of Proto planetary-nebulae [5–7].

The prominent 3.3 $\mu m$ band depends not only on the charge states of PAHs but also on the size and structure. In neutrals the intensity of this band increases with the PAH size. AIB observations and comparison with PAH spectral data has led to the conclusion that smaller PAHs give rise to this 3.3 $\mu m$ band while all the other features are from comparatively larger PAHs [34,36]. While PAH cations are less likely to contribute to this mode, the intensity probably comes from neutrals and anions [53].

The $C-H$ out of plane bend modes depend mainly on the edge structure of the emitting PAHs. The intensities and positions of various peaks for these features depend on the number of adjacent hydrogen atoms on the periphery of the PAH ring [54]. In cations these bands are blue shifted. The most prominent

[48] and hence probably the most abundant is the solo hydrogen mode (11.2 $\mu m$ mode). As the PAH size and compactness increases the number of solo hydrogens increases and hence the intensity of this mode.

A comparison between the co-added spectra of catacondensed PAHs [23] with the pericondensed PAHs is shown in Fig. 8 & 9. The cations of both class have intense bands in the 1100 – 1600 $cm^{-1}$ region. The 6.2 $\mu m$ AIB shows good frequency match with neutral PAHs but has a better intensity corelation with cations. In cations this band is red shifted away from the AIB, but is again blue shifted close to the AIB as the size of the cation grows. It has been previously suggested [55] that PAH cations having 50 - 80 C atoms may be the carriers of 1610 $cm^{-1}$ AIB and features redder to it may be carried by smaller (20 - 40 C atoms) PAHs. In $C_{28}H_{14}$ cation the 1592 $cm^{-1}$ peak correlates very well with the class $B$ [7] 6.3 $\mu m$ AIB. A recent study [56] reports that shortest wavelength of this AIB can be reproduced by compact PAHs having nitrogen substituted deep within their structure. Neutral PAHs like perylene and bisanthene, having bay regions in their structure, and fluoranthenes [57] show intense band around 1600 $cm^{-1}$. Such structures may also contribute to the 6.2 $\mu m$ AIB.

The intensities as well as band position matching with the interstellar AIBs is better for pericondensed PAHs than for catacondensed PAHs. The enlarged co-added spectra (Fig. 9) shows that catacondensed PAH cations showed three sharp peaks in the 1100 – 1600 $cm^{-1}$ region [23], while the AIBs have a broad feature near 1300 $cm^{-1}$. Pericondensed PAH cations present a better agreement in this regard with the 7.7 $\mu m$ AIB. Observational studies suggest that the 7.7 $\mu m$ feature is complex and consists of at least two subcomponents at 7.6 and 7.8 $\mu m$ and some sources are found to exhibit more sub features at 7.4

$\mu m$ and 8.2 $\mu m$ [6,7]. Summation of all these features result in a broad emission plateau at 7.7 $\mu m$. The cumulative spectra of all pericondensed cations Fig. 9(b) shows two plateaus, nearly equal in intensity, are present at 1285 and 1315 $cm^{-1}$ resulting in a broad 1300 $cm^{-1}$ feature. The profile of this mode shows good match with the AIB profile of NGC-2023 and other similar objects catagorized as $A'$ profile [7]. These $A'$ profiles are from objects having star formation activity - HII regions, reflection nebulae and extra galactic sources. Star forming regions have intense background radiation increasing the possibility of PAH cations [5].

Recently some new infrared emission features have been detected at 6.7, 10.1, 15.8, 17.4 and 19.0 $\mu m$ by the Spitzer Space Telescope [58]. Possible identifications include different modes of aromatic hydrocarbons. The study of 15 – 20 $\mu m$ region has suggested few PAH cations to be contributing to the 19.0 $\mu m$ band [59]. The 15 – 20 $\mu m$ plateau results not only from the emissions from individual PAHs, but PAH clusters, amorphous carbon particles and other PAH related species could contribute as well. While individual PAHs seem to be responsible for the sharp features at 16.4 and 17.4 $\mu m$ (610 and 575 $cm^{-1}$), emissions from PAH clusters could contribute to the broad structureless underlying plateau between 15 and 20 $\mu m$ (670 and 500 $cm^{-1}$) [59]. We note that the computed spectra of pericondensed PAH cations do show a feature at 545 $cm^{-1}$ which could correspond to the newly detected peak at 19.0 $\mu m$ along with a broad plateau between 500 – 700 $cm^{-1}$ (Fig. 8).

## 6 Conclusions

The charge distribution of small to medium sized pericondensed PAHs in neutral and cationic forms have been studied. The intensity changes in case of PAH ions are discussed and related to the changes occuring in the charge distribution. The charge on the hydrogen atoms has an inverse relation with $C-H$ stretch intensity. As the positive charge on the hydrogen atom increases, the $C-H$ stretch intensity is highly reduced and vice-versa. The $C-C$ stretch and $C-H$ in plane bend mode intensities in the cations increase and mostly it is the change in charge of outer carbon atoms that seem to be responsible. The charge changes upon ionization of PAHs produce high intensities in the 1100 – 1600 $cm^{-1}$ region for both cations and anions. This indicates that the neutral charge distribution is unique and any departure from it increases the intensity of these modes.

The charge change may be induced by ionization, by substitution, by hetero-atom addition or any other structural change.

The spectra of studied pericondensed PAHs is largely independent of the size and structure of molecules except for a few small variations. The variation in spectra in relation to size may be better understood by a study of much larger PAHs and may further help in narrowing down the possible PAHs inhabiting the ISM. Pericondensed PAHs give a better correlation with the AIBs and the band shifts and intensity variations indicate towards the possibility of larger species in the ISM. For the 7.7 $\mu m$ AIB, the composite spectra of studied pericondensed PAH cations show position and profile similarity with observed $A'$ profile in objects having star formation activity. The IR information of a

large number of PAHs in various charged states shall be useful in modelling the complete AIB spectrum in different environments. This shall help in quantifying the amount of UV flux present in the astrophysical regions and thus lead to a better understanding of the astrophysical object.

## Acknowledgements

The authors acknowledge the use of computational and library facilities at Inter University Centre for Astronomy and Astrophysics, Pune. AP acknowledges receipt of fellowship from University Grants Commission, New Delhi. The insightful comments and suggestions of the refrees are thankfully acknowledged.

## References

[1] M. Cohen, A.G.G.M. Tielens, J.D. Bregman, F.C. Witteborn, D.M. Rank, L.J. Allamandola, D. Wooden, M. de Muizon, Astrophys. J. 341 (1989) 246.

[2] T.R. Geballe, A.G.G.M. Tielens, L.J. Allamandola, A. Moorhouse, P.W.J.L. Brand, Astrophys. J. 341 (1989) 278.

[3] J.D. Bregman, L.J. Allamandola, A.G.G.M. Tielens, T.R. Geballe, F.C. Witteborn, Astrophys. J. 344 (1989) 791.

[4] First ISO Results, Astron. Astrophys. 315 (1996) L26 - L400.

[5] L.J. Allamandola, D.M. Hudgins, S.A. Sandford, Astrophys. J. 511 (1999) L115.

[6] E. Peeters, L.J. Allamandola, D.M. Hudgins, S. Hony, A.G.G.M. Tielens, in: A.N. Witt, G.C. Clayton, B.T. Draine (Eds.) ASP Conf. Ser., Astrophysics of Dust, (San Francisco: ASP) 309 (2003) p. 141.

[7] E. Peeters, S. Hony, C. Van Kerckhoven, A.G.G.M. Tielens, L.J. Allamandola, D.M. Hudgins, C.W. Bauschlicher, Astron. Astrophys, 390 (2002) 1089.

[8] A. Leger, J.L. Puget, Astron. Astrophys. 137 (1984) L5.

[9] L.J. Allamandola, A.G.G.M. Tielens, J.R. Barker, Astrophys. J. 290 (1985) L25.

[10] L.J. Allamandola, A.G.G.M. Tielens, J.R. Barker, Astrophys. J. Supp. Ser. 71 (1989) 733.

[11] J.L. Puget, A. Leger, Ann. Rev. Astron. Astrophys. 27 (1989) 161.

[12] C. Joblin, A. Leger, P. Martin, Astrophys. J. 393 (1992) L79.

[13] G.C. Clayton, K.D. Gordon, F. Salama, L.J. Allamandola, P.G. Martin, T.P. Snow, D.C.B. Whittet, A.N. Witt, M.J. Wolff, Astrophys. J. 592 (2003) 947.

[14] G.P. van der Zwet, L.J. Allamandola, Astron. Astrophys. 146 (1985) 76.

[15] A.G.G.M. Tielens, T.P. Snow, The Diffuse Interstellar Bands, Kluwer, 1995.

[16] F. Salama, E. Bakes, L.J. Allamandola, A.G.G.M. Tielens, Astrophys. J. 458 (1996) 621.

[17] J. Szczepanski, M. Vala, Nature 363 (1993) 699.

[18] H.S. Kim, R.J. Saykally, Astrophys. J. Supp. Ser., 143 (2002) 455.

[19] H.S. Kim, D.R. Wagner, R.J. Saykally, Phys. Rev. Lett. 86 (2001) 5691.

[20] D.J. Cook, S. Schlemmer, N. Balucani, D.R. Wagner, B. Stelner, R.J. Saykally, Nature 380 (1996) 227.

[21] S.R. Langhoff, J. Phys. Chem. 100 (1996) 2819.

[22] C.W. Bauschlicher Jr, E.L.O. Bakes, Chem. Phys. 262 (2000) 285.

[23] A. Pathak, S. Rastogi, Chem. Phys. 313 (2005) 133.

[24] D.J. De Frees, M.D. MIller, D. Talbi, F. Pauzat, Y. Ellinger, Astrophys. J. 408 (1993) 530.

[25] F. Pauzat, D. Talbi, M.D. Miller, Y. Ellinger, Astron. Astrophys. 293 (1995) 263.

[26] F. Pauzat, D. Talbi, M.D. Miller, Y. Ellinger, Astron. Astrophys. 319 (1997) 318.

[27] F. Pauzat, Y. Ellinger, Chem. Phys. 280 (2002) 267.

[28] C.W. Bauschlicher, Astrophys. J. 564 (2002) 782.

[29] S.R. Langhoff, C.W. Bauschlicher, D.M. Hudgins, S.A. Sandford, L.J. Allamandola, J. Phys. Chem. A 102 (1998) 1632.

[30] C.W. Bauschlicher, Chem. Phys. 234 (1998) 87.

[31] D.M. Hudgins, S.A. Sandford, J. Phys. Chem. A 102 (1998) 394.

[32] D.M. Hudgins, L.J. Allamandola, J. Phys. Chem. 99 (1995) 3033.

[33] M. Vala, J. Szczepanski, F. Pauzat, O. Parisel, D. Talbi, Y. Ellinger, J. Phys. Chem. 98 (1994) 9187.

[34] W.A. Schutte, A.G.G.M. Tielens, L.J. Allamandola, Astrophys. J. 415 (1993) 397.

[35] E.L.O. Bakes, A.G.G.M. Tielens, C.W. Bauschlicher, Astrophys. J. 556 (2001) 501.

[36] C. Pech, C. Joblin, P. Boissel, Astron. Astrophys. 388 (2002) 639.

[37] T. Allain, S. Leach, E. Sedlmayr, Astron. Astrophys. 305 (1996) 616.

[38] V. Le Page, T.P. Snow, V.M. Bierbaum, Astrophys. J. 584 (2003) 316.

[39] GAMESS, M.W. Schmidt, K.K. Baldridge, J.A. Boatz, S.T. Elbert, M.S. Gordon, J.H. Jensen, S. Koseki, N. Matsunaga, K.A. Nguyen, S.J. Su, T.L. Windus, M. Dupuis, J.A. Montgomery, J. Comput. Chem. 14 (1993) 1347.

[40] C.W. Bauschlicher, S.R. Langhoff, Spectrochim. Acta A 53 (1997) 1225.

[41] J. M. L. Martin, J. El-Yazal, and J.P. Francois, J. Phys. Chem. 100 (1996) 15358.

[42] H. Yoshida, A. Ehara, H. Matsuura, Chem. Phys. Lett. 325 (2000) 477.

[43] F. Jensen, Computational Chemistry, Chap. 9, John Wiley and Sons, 2001.

[44] G. Herzberg, Molecular Spectra and Molecular Structure, Electronic Spectra and Electronic Structure of Polyatomic Molecules, Van Nostrand, New York, (1966).

[45] C.W. Bauschlicher, D.M. Hudgins, L.J. Allamandola, Theor. Chem. Acc. 103 (1999) 154.

[46] J. Oomens, B.G. Sartakov, A.G.G.M. Tielens, G. Meijer, G. von Helden, Astrophys. J. 560 (2001) L99.

[47] D.M. Hudgins, C.W. Bauschlicher Jr, L.J. Allamandola, Spectrochim. Acta A 57 (2001) 907.

[48] C. Joblin, L. d'Hendecourt, A. Leger, D. Defourneau, Astron. Astrophys. 281 (1994) 923.

[49] S. Hony, C. van Kerckhoven, E. Peeters, A.G.G.M. Tielens, D.M. Hudgins, L.J. Allamandola, Astron. Astrophys, 370 (2001) 1030.

[50] D.J. Cook, S. Schlemmer, N. Balucani, D.R. Wagner, J.A. Harrison, B. Steiner, R.J. Saykally, J. Phys. Chem. A 102 (1998) 1465.

[51] C. Joblin, D. Toublanc, P. Boissel, A.G.G.M. Tielens, Mol. Phys. 100 (2002) 3595.

[52] G. Mulas, G. Malocci, C. Joblin, D. Toublanc, Astron. Astrophys. 446 (2006) 537.

[53] B. van Diedenhoven, E. Peeters, C. van Kerckhoven, S. Hony, D.M. Hudgins, L.J. Allamandola, A.G.G.M. Tielens, Astrophys. J. 611 (2004) 928.

[54] D.M. Hudgins, L.J. Allamandola, Astrophys. J. 516 (1999) L41.

[55] D.M. Hudgins, L.J. Allamandola, Astrophys. J. 513 (1999) L69.

[56] D.M. Hudgins, C.W. Bauschlicher, L.J. Allamandola, Astrophys. J. 632 (2005) 316.

[57] D.M. Hudgins, C.W. Bauschlicher, L.J. Allamandola, J.C. Fetzer, J. Phys. Chem. A 104 (2000) 3655.

[58] M.W. Werner, K.L. Uchida, K. Sellgren, M. Marengo, K.D. Gordon, P.W. Morris, J.R. Houck, J.A. Stansberry, Astrophys. J. Supp. Ser. 154 (2004) 309.

[59] E. Peeters, A.L. Mattioda, D.M. Hudgins, L.J. Allamandola, Astrophys. J. 617 (2004) L65.

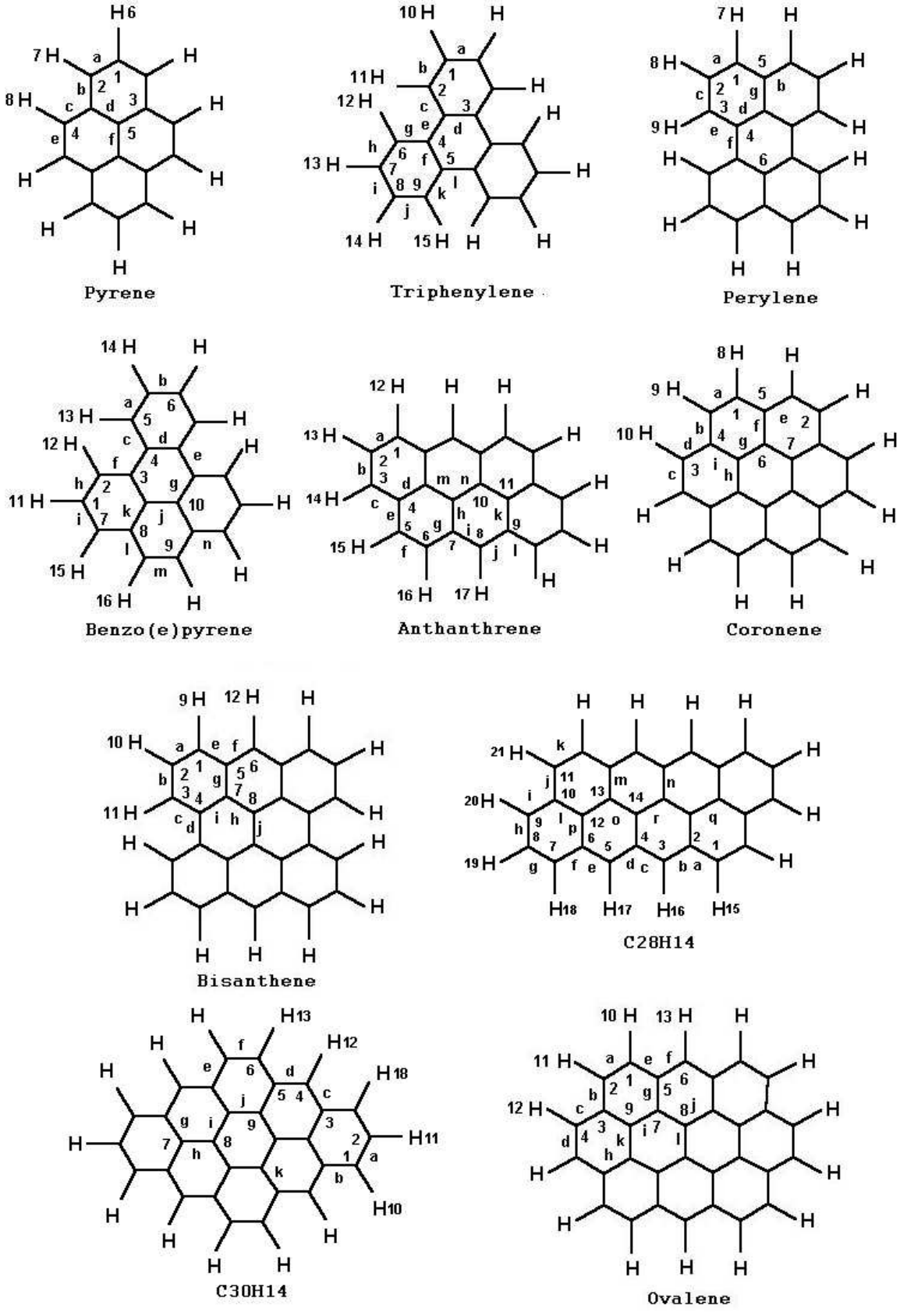


Fig. 1. Pericondensed PAHs; symmetry unique atoms and bonds are labelled.

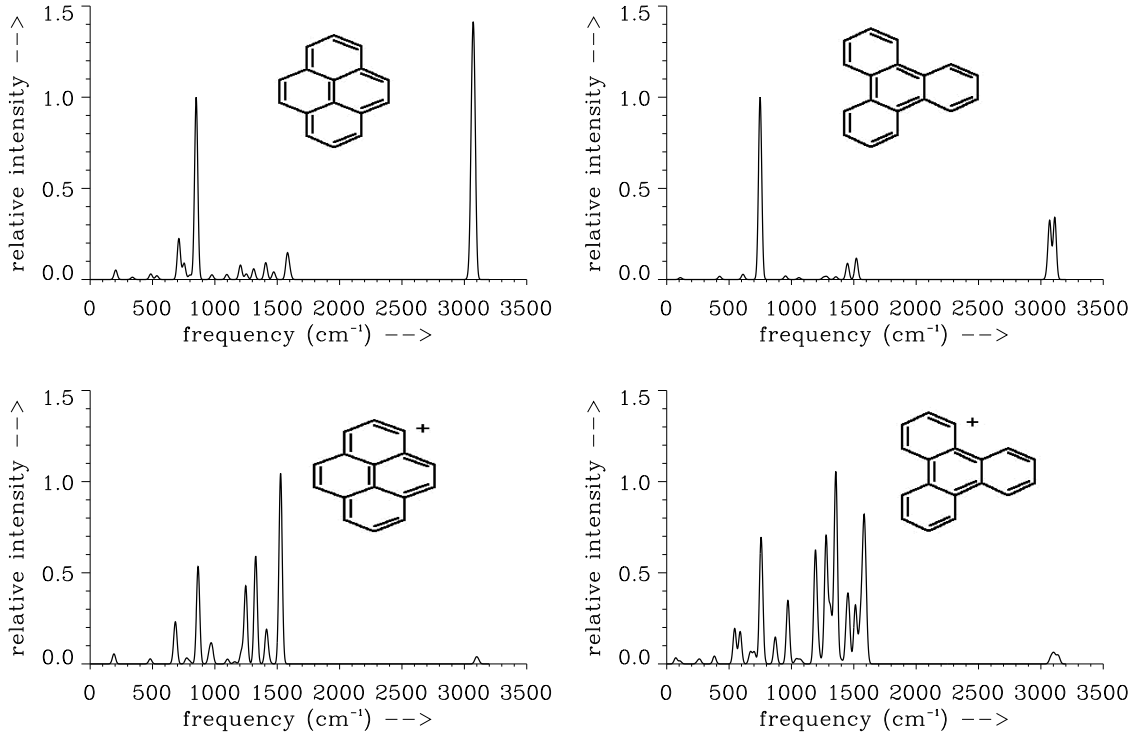


Fig. 2. Infrared spectra of Pyrene and Triphenylene.

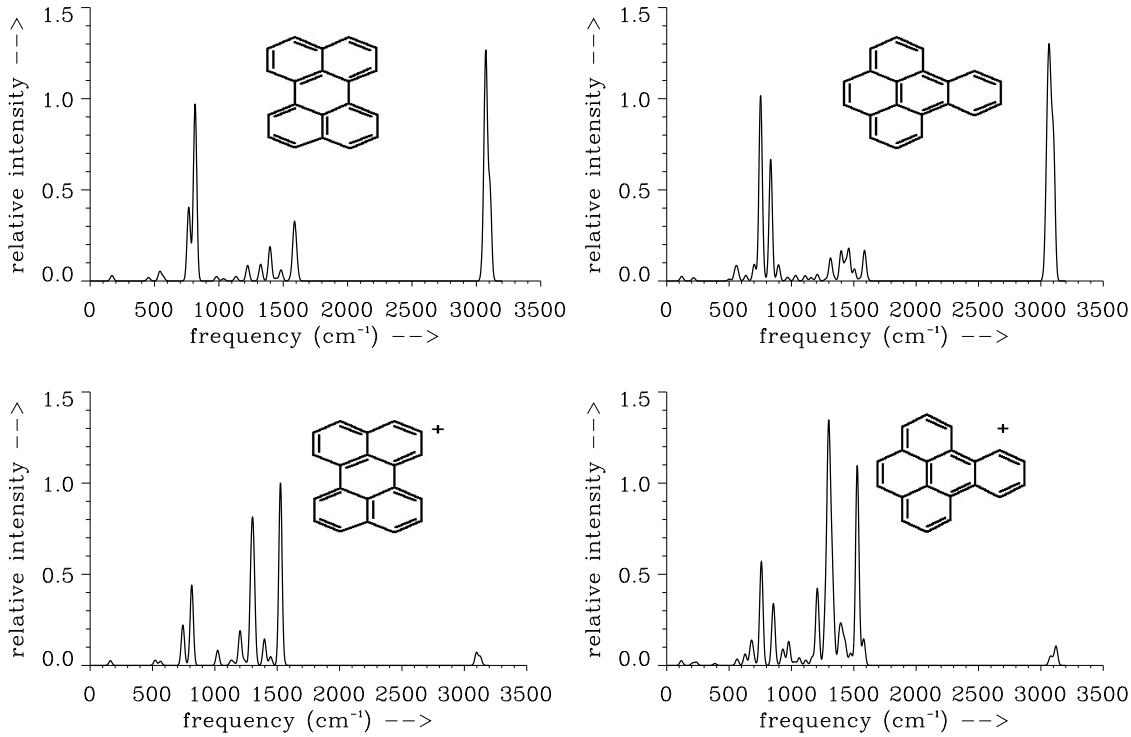


Fig. 3. Infrared spectra of Perylene and Benzo(e)pyrene.

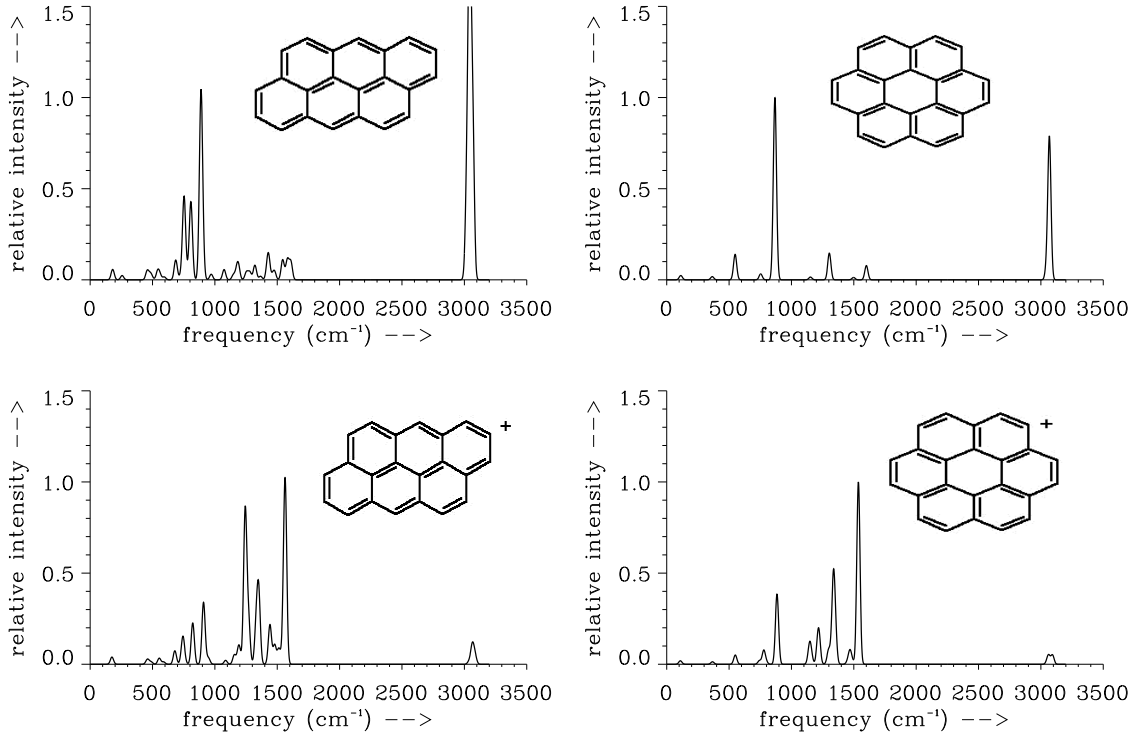


Fig. 4. Infrared spectra of Anthanthrene and Coronene.

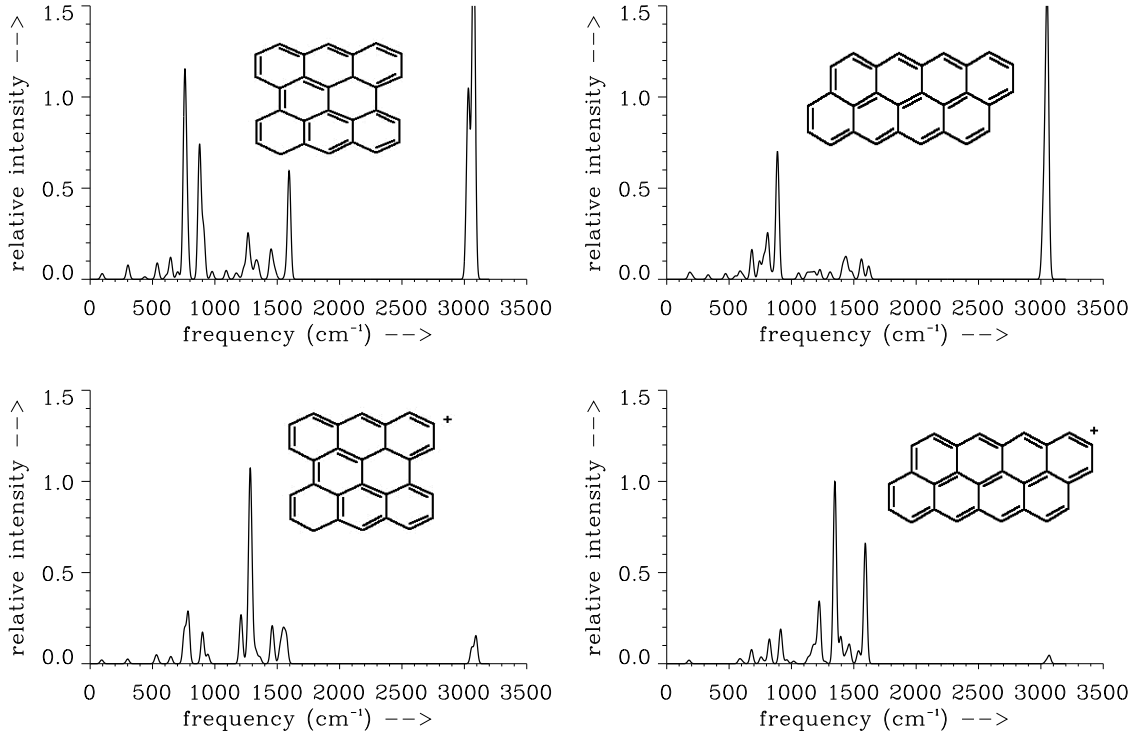


Fig. 5. Infrared spectra of Bisanthene and $C_{28}H_{14}$.

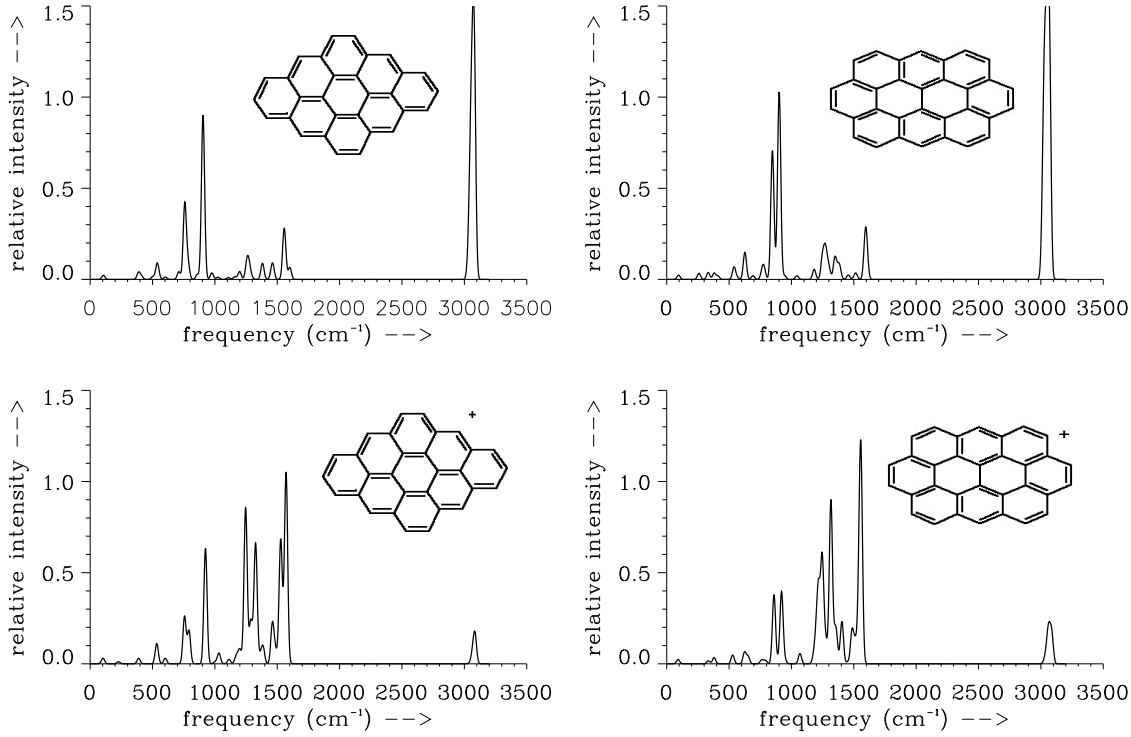


Fig. 6. Infrared spectra of $C_{30}H_{14}$ and Ovalene.

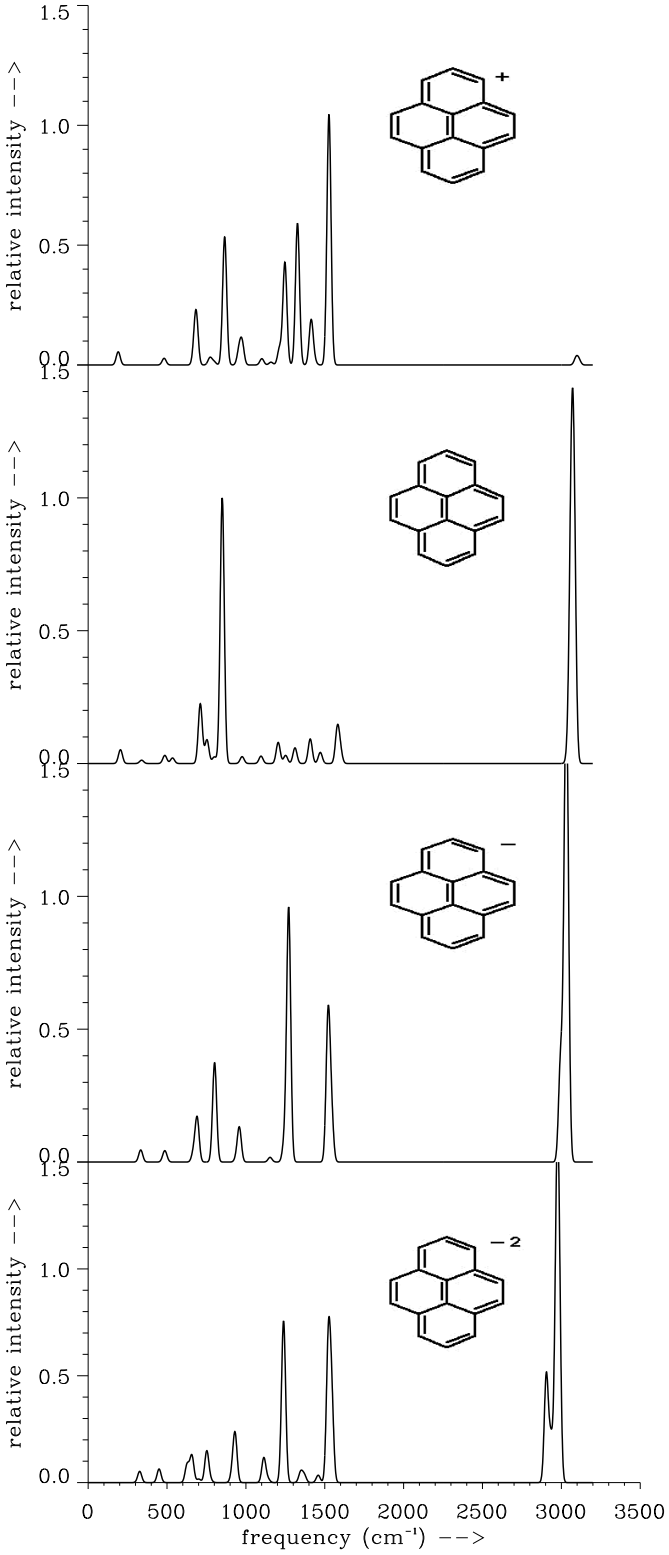


Fig. 7. Comparison of infrared spectra of various charge states of Pyrene.

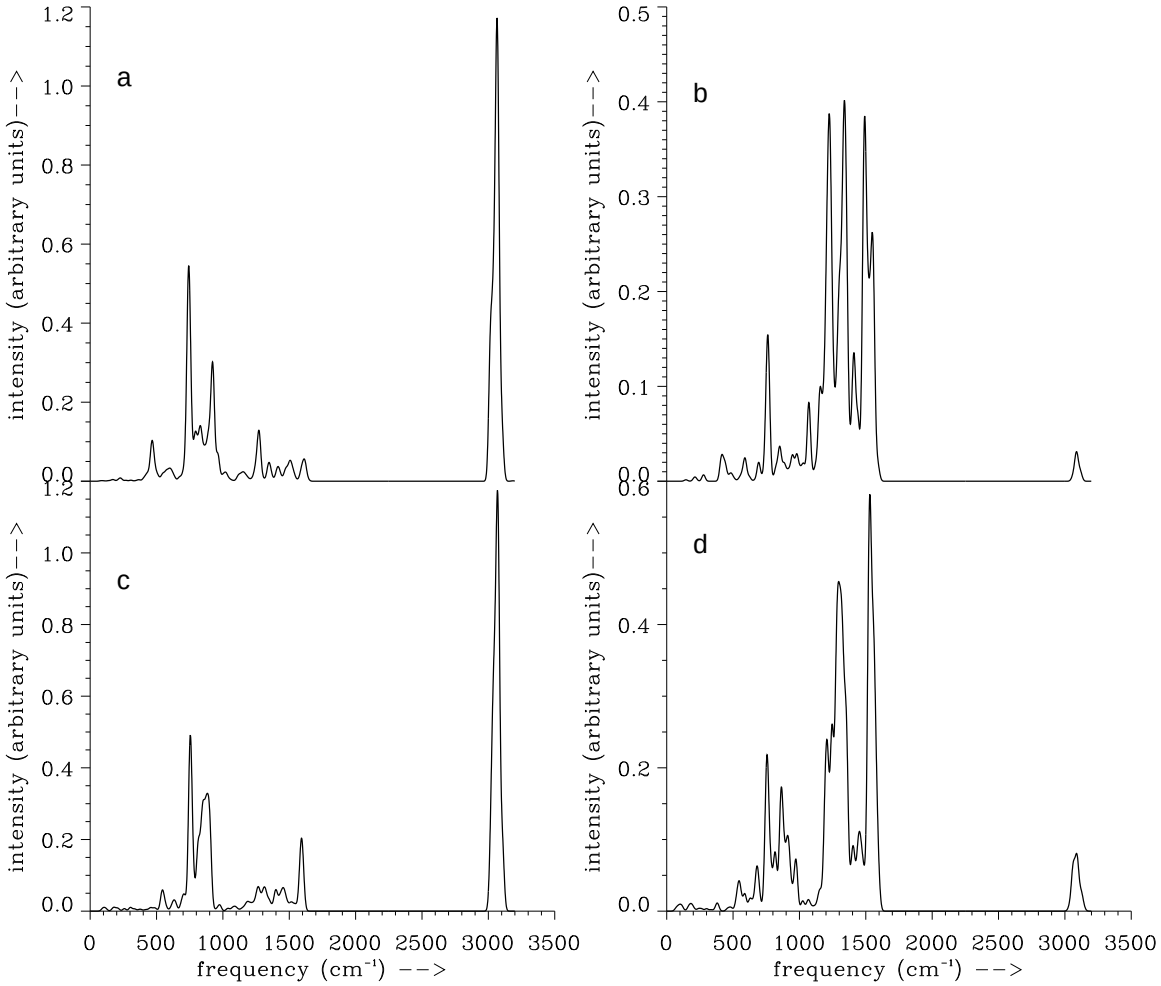


Fig. 8. Co–added spectra of PAHs in equal proportion : (a) studied neutral Catacondensed PAHs, (Ref. 22), (b) studied Catacondensed PAH cations, (Ref. 22) (c) studied neutral Pericondensed PAHs in this work and (d) studied Pericondensed PAH cations in this work.

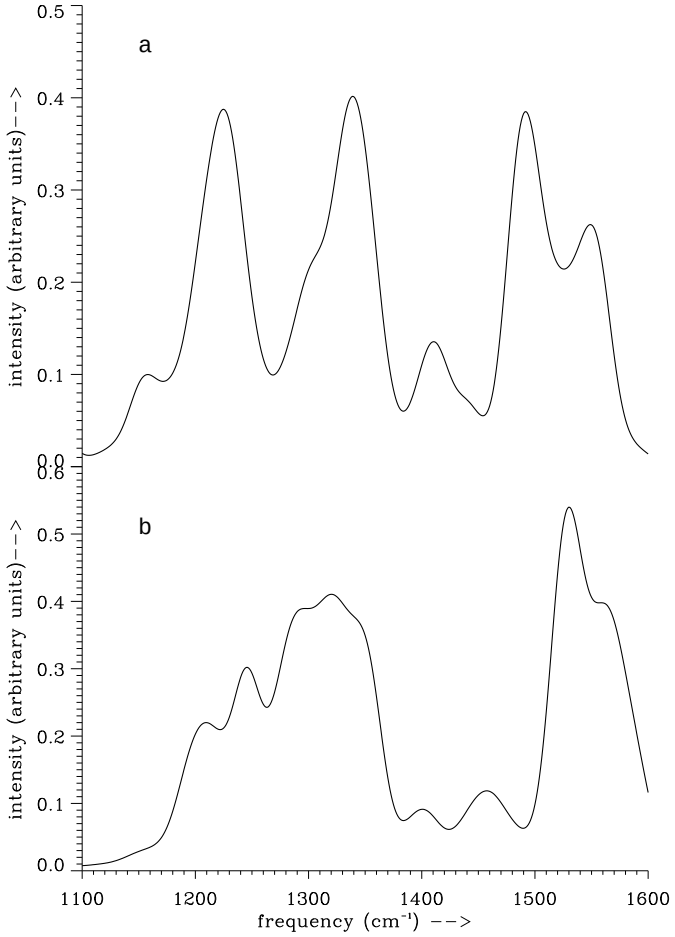


Fig. 9. Comparison of the 1100 to 1600 $cm^{-1}$ region of the calculated co-added spectra (a) Catcondensed PAH cations (b) Pericondensed PAH cations. The 1300 $cm^{-1}$ feature is seen to be composed of two different peaks at 1285 and 1315 $cm^{-1}$.